Density functional study of the phase behavior of asymmetric binary dipolar mixtures

Gabriel M. Range* and Sabine H. L. Klapp†
Stranski-Laboratorium für Physikalische und Theoretische Chemie, Sekretariat TC 7, Fakultät II für Mathematik und Naturwissenschaften, Technische Universität Berlin, Straße des 17. Juni 124, D-10623 Berlin, Germany
(Received 5 November 2003; published 26 April 2004)

Using density functional theory in the modified mean-field (MMF) approximation we study the phase behavior of asymmetric binary mixtures of equisized dipolar hard spheres with different dipole moments in the fluid phase regime. We focus on "dipole-dominated" systems where isotropic attractive interactions are absent. Despite these restrictions our results reveal complex fluid-fluid phase behavior involving demixing and first- and second-order isotropic-to-ferroelectric phase transitions the relative importance of which depends on two "tuning" parameters, that is, the parameter Γ measuring the ratio of the dipolar coupling strengths, and the chemical potential difference $\Delta\mu$ controlling the composition. The interplay of these effects then yields three different types of phase behavior differing in the degree to which demixing dominates the system. A generic feature of the resulting diagrams is that the isotropic-to-ferroelectric transition is shifted towards significantly higher densities compared to the one-component case, and is therefore destabilized. Furthermore, demixing in the MMF approach turns out to be always accompanied by spontaneous ferroelectricity, which is in contrast to recent integral equation and simulation results for the limiting case of a mixture of dipolar and pure hard spheres ($\Gamma=0$).

DOI: 10.1103/PhysRevE.69.041201 PACS number(s): 61.20.−p, 77.80.−e, 64.70.−p, 61.25.Em

I. INTRODUCTION

Understanding phase properties of fluid mixtures whose components carry permanent dipole moments is important in various contexts. For example, molecular polar mixtures are intrinsically interesting as solutes since their solvation properties can be tuned by varying the composition [1,2]. In order to make use of these properties, however, it is vital to know under which thermodynamic conditions the mixtures demix and/or condensate. Another example are ferrocolloids [3,4] which are usually polydisperse and can therefore be regarded as (multicomponent) dipolar mixtures as well [5,6]. Depending on details of the colloidal stabilizing procedure and on external conditions (e.g., presence of an external field), ferrocolloids can exhibit both condensation and demixing transitions, where the latter are particularly important as a method to size separate the system. Despite these motivations, there are so far only few theoretical studies [7–9] on the phase behavior of such mixtures, partly because the treatment of the long-range anisotropic dipolar interactions in computer simulations and other theoretical approaches is still involved. Consequently, a more precise understanding of the link between the mixture's microscopic features such as presence of dipolar interactions of various strengths, van der Waals-like forces, size asymmetry between the components, etc., and the macroscopic phase behavior, e.g., the appearance of a demixing transition, is still missing.

The purpose of the present work is to contribute to fill this gap by an investigation of one of the most simple models for a dipolar mixture, that is, a binary mixture of equisized dipolar hard spheres (DHS) with different dipole moments (in zero field). Choosing this somewhat minimalistic model, which lacks any dispersive interactions or asymmetric steric interactions due to different sizes of the spheres, thus permits us to study directly the influence of dipolar interactions on the mixture's phase behavior. In fact, recent research on *one-component* DHS fluids (and related model systems) has demonstrated that the long-range and highly anisotropic character of dipolar interactions yields new, unexpected phase behavior [10–14], including the possibility of *spontaneous polarization* in dense, strongly coupled DHS fluids [15–22]. In view of these findings, central topics of the present study are the appearance of such ferroelectric phases in two-component fluids, and their interplay with *demixing* transitions expected to take place for highly asymmetric mixtures.

We address these questions using density functional theory in the so-called modified mean-field (MMF) approximation, where the pair correlation function g is replaced by the Boltzmann factor (contrary to simple mean-field theory, where g is set to one). The same ansatz has been previously employed to study phase properties of one-component dipolar fluids [19,20] and fluids with spin-dependent interactions such as Heisenberg spin fluids [27]. Regarding the performance of MMF theory for dipolar fluids, results obtained so far [19–21,23–25] suggest that the theory does reproduce main features of the phase behavior such as the appearance of spontaneous polarization and the presence (absence) of ordinary condensation transitions in pure Stockmayer (DHS) fluids, whereas more subtle features such as dipolar chain formation observed in computer simulation studies of highly diluted dipolar systems [10–12,14] are not captured by the approach. On the other hand, the great advantage of MMF theory (compared to computer simulations or other liquid-state approaches such as integral equation theories) is that it is simple to apply and thereby allows to quickly scan phase diagrams for large portions of the parameter space. Thus, the approach seems to be particularly useful to get a first idea of

*Electronic address: gabriel.range@fluids.tu-berlin.de
†Electronic address: sabine.klapp@fluids.tu-berlin.de

the influence of different dipolar interactions on the mixture's phase behavior.

The rest of the paper is organized as follows. In Sec. II we formulate our model and derive the MMF expression for the free energy functional, focussing on *fluid* phases with isotropic or orientationally ordered character (Sec. II A). The resulting functional is a generalization of the corresponding expression for pure dipolar systems derived earlier in Ref. [19,20]. After defining conditions for phase equilibria (Sec. II B) we also present in Sec. II C an appropriate stability analysis which allows us to locate critical lines of the mixture. Results are presented in Sec. III where we start by briefly recalling the one-component system and subsequently discuss in Sec. III C different types of (density-temperature and concentration-temperature) phase diagrams obtained for dipolar mixtures. The topology of these diagrams turns out to depend both on the interaction parameter Γ (which measures the ratio of the dipolar coupling strengths) and on the chemical potential difference $\Delta\mu$ controlling the composition. To complete the picture we also present our results in the density-concentration plane (Sec. III D), which turned out to be a particularly useful representation to identify differences between the various phase properties observed. Finally, our conclusions are summarized in Sec. IV.

II. MODEL AND METHOD

We consider a binary mixture of two species (A and B) of dipolar hard spheres with equal diameters σ but different dipole moments m_A and m_B. The pair potential for two of such particles at positions $\mathbf{r}_1$ and $\mathbf{r}_2$ is given by

$$u_{ab}(\mathbf{r}_{12},\omega_1,\omega_2) = u^{\mathrm{hs}}(r_{12}) + u^{\mathrm{dip}}_{ab}(\mathbf{r}_{12},\omega_1,\omega_2), \qquad (2.1)$$

where $r_{12}=|\mathbf{r}_{12}|=|\mathbf{r}_2-\mathbf{r}_1|$ is the particle separation, $\omega=(\theta,\phi)$ represents the orientation of a dipole in a spatially fixed coordinate system, and the subscripts a and b denote the components considered $[a(b)=\mathrm{A},\mathrm{B}]$. The repulsive hard sphere interaction and the dipolar interaction are given by

$$u^{\mathrm{hs}}(r_{12}) = \begin{cases} \infty, & r_{12}<\sigma \\ 0, & r_{12}>\sigma, \end{cases} \qquad (2.2)$$

and

$$u^{\mathrm{dip}}_{ab}(\mathbf{r}_{12},\omega_1,\omega_2) = \frac{m_a m_b}{r_{12}^3}[\hat{\mathbf{m}}(\omega_1)\cdot\hat{\mathbf{m}}(\omega_2) - 3[\hat{\mathbf{m}}(\omega_1)\cdot\hat{\mathbf{r}}_{12}][\hat{\mathbf{m}}(\omega_2)\cdot\hat{\mathbf{r}}_{12}]], \qquad (2.3)$$

where $\hat{\mathbf{m}}(\omega)$ is a unit vector in direction of ω and $\hat{\mathbf{r}}_{12}=\mathbf{r}_{12}/r_{12}$.

In the present work we limit ourselves to the treatment of spatially homogeneous, but possibly orientationally ordered phases. Solidlike structures or domain formation are thus neglected and the singlet density of the system can be written as

$$\rho_a(\mathbf{r},\omega) = \rho_a\alpha_a(\omega), \qquad \int d\omega\alpha_a(\omega) = 1. \qquad (2.4)$$

In Eq. (2.4) $\alpha_a(\omega)$ is the orientational distribution function, which is normalized to one. For isotropic states the orientational distribution is constant, that is, $\alpha_a(\omega)=1/(4\pi)$. Deviations from that value indicate the presence of orientational order, which, for the states considered, can be expected to be axially symmetric. As a result, $\alpha_a(\omega)$ can be expressed via an expansion in Legendre polynomials $\mathcal{P}_l$,

$$2\pi\alpha_a(\omega) = \overline{\alpha}_a(\cos\,\theta) = \frac{1}{2} + \sum_{l=1}^{\infty}\alpha_{a,l}\mathcal{P}_l(\cos\,\theta), \qquad (2.5)$$

where the expansion coefficients $\alpha_{a,l}$ are connected to the order parameters $P_{a,l}$ by

$$P_{a,l} = \int_{-1}^{1} dx\overline{\alpha}_a(x)\mathcal{P}_l(x) = \frac{2}{2l+1}\alpha_{a,l}. \qquad (2.6)$$

With these definitions, the isotropic phase is specified by $P_{a,l\geqslant 1}=0$, i.e., $\overline{\alpha}_a(x)=1/2$, whereas a phase with nematic orientational order would be characterized by $P_{a,l}=0(\neq 0)$ for odd (even) l, i.e., $\overline{\alpha}_a(x)=\overline{\alpha}_a(-x)$. Finally, if $P_{a,l}\neq 0$ for all l, the system is in a ferroelectric phase.

A. Modified mean-field theory

The two main difficulties arising in theoretical treatments of dipolar fluids are the angle dependence of the dipolar potential on one hand, and it's long-range character on the other hand. In the present work we treat these problems in the framework of a density functional approach, which is a generalization of an earlier study by Groh and Dietrich [19,20] on one-component dipolar fluids.

We start by considering the free energy $F=F^{\mathrm{id}}+F^{\mathrm{hs}}+F^{\mathrm{dip}}$ of the mixture which can be separated into the ideal gas part (F^{id}), the hard sphere excess part (F^{hs}), and a part which stems from the dipolar interaction (F^{dip}). The ideal part is given by

$$\frac{F^{\mathrm{id}}}{\mathcal{V}} = \sum_a \frac{\rho_a}{\beta}[\ln(\rho_a\Lambda_a^3)-1] + \sum_a \frac{\rho_a}{\beta}\int_{-1}^{1} dx\overline{\alpha}_a(x)\ln(2\overline{\alpha}_a(x)), \qquad (2.7)$$

where $\mathcal{V}$ is the volume, Λ_a is the thermal wavelength, and $\beta=1/k_\mathrm{B}T$ is the inverse temperature. The second term in Eq. (2.7) accounts for the loss of entropy in anisotropic configurations [it vanishes for $\overline{\alpha}_a(x)=1/2$].

As to the hard-sphere excess part, it is sufficient to use a one-component approximation, since we are dealing solely with equally sized species in this work. We choose the Carnahan-Starling expression [26]

$$\frac{F^{\mathrm{hs}}}{\mathcal{V}} = \frac{\rho}{\beta}\frac{4\eta-3\eta^2}{(1-\eta)^2}, \qquad (2.8)$$

where the packing fraction $\eta=(\pi/6)\rho\sigma^3$ depends on the total number density $\rho=\rho_\mathrm{A}+\rho_\mathrm{B}$.

Finally, the dipolar contribution F^{dip} is treated in the

framework of the *modified mean-field* approximation where the pair distribution function is set to its low-density limit, i.e.,

$$g_{ab}(\mathbf{r}_{12},\omega_1,\omega_2)=\exp(-\beta u_{ab}(\mathbf{r}_{12},\omega_1,\omega_2)). \tag{2.9}$$

With this simplification, one can derive analogous to the one-component case [27–30]

$$F^{\mathrm{dip}}=-\frac{1}{2\beta}\sum_{ab}\int d\mathbf{r}_1 d\omega_1 d\mathbf{r}_2 d\omega_2 \rho_a(\mathbf{r}_1,\omega_1)\rho_b(\mathbf{r}_2,\omega_2) \times\exp(-\beta u^{\mathrm{hs}}(r_{12}))f_{ab}^{\mathrm{dip}}(\mathbf{r}_{12},\omega_1,\omega_2), \tag{2.10}$$

where

$$f_{ab}^{\mathrm{dip}}(\mathbf{r}_{12},\omega_1,\omega_2)=\exp(-\beta u_{ab}^{\mathrm{dip}}(\mathbf{r}_{12},\omega_1,\omega_2))-1 \tag{2.11}$$

is the Mayer function. To simplify the expression for F^{dip} we rewrite the dipole potential in rotationally invariant form,

$$u_{ab}^{\mathrm{dip}}(\mathbf{r}_{12},\omega_1,\omega_2)=\frac{m_a m_b}{r_{12}^3}\tilde{\Phi}_{112}(\omega_1,\omega_2,\omega_{12}), \tag{2.12}$$

where ω_{12} describes the orientation of $\mathbf{r}_{12}$, and

$$\tilde{\Phi}_{112}(\omega_1,\omega_2,\omega_{12})=-(4\pi)^{3/2}\sqrt{\frac{2}{15}}\Phi_{112}(\omega_1,\omega_2,\omega_{12}) \tag{2.13}$$

is a rotational invariant, the general expression for which is given by [31]

$$\Phi_{l_1 l_2 l}(\omega_1,\omega_2,\omega_{12})=\sum_{m_1 m_2 m}C(l_1 l_2 l;m_1 m_2 m) \times Y_{l_1 m_1}(\omega_1)Y_{l_2 m_2}(\omega_2)Y_{lm}^{*}(\omega_{12}). \tag{2.14}$$

In Eq. (2.14), the $C(l_1 l_2 l;m_1 m_2 m)$ are Clebsch-Gordan coefficients and $Y_{lm}(\omega)$ are spherical harmonics.

In order to express the Mayer function, Eq. (2.11), in rotational invariants we employ a Taylor expansion in powers of $-\beta u^{\mathrm{dip}}$, yielding

$$f_{ab}^{\mathrm{dip}}(\mathbf{r}_{12},\omega_1,\omega_2)=\sum_{n=1}^{\infty}\frac{1}{n!}\left(\frac{-\beta m_a m_b}{r_{12}^3}\right)^n\tilde{\Phi}_{112}^n(\omega_1,\omega_2,\omega_{12}). \tag{2.15}$$

Inserting Eq. (2.15) and expressions (2.4) and (2.5) for the singlet density into the MMF expression of F^{dip} (2.10), it can be written as a quadratic form in the density coefficients appearing in Eq. (2.5), that is,

$$\frac{F^{\mathrm{dip}}}{\mathcal{V}}=\sum_{ab}\rho_a\rho_b\sum_{l,m=0}^{\infty}\tilde{u}_{ab,lm}\alpha_{a,l}\alpha_{b,m}, \tag{2.16}$$

with

$$\alpha_{a,0}=1/2, \tag{2.17}$$

which is still exact within the MMF approximation. The quantities $\tilde{u}_{ab,lm}$ appearing in Eq. (2.16) are defined by

$$\tilde{u}_{ab,lm}=\sum_{n=1}^{\infty}\tilde{u}_{lm}^{(n)}(m_a m_b)^n, \tag{2.18}$$

where the $\tilde{u}_{lm}^{(n)}$ are temperature-dependent coefficients resulting from the integrals in Eq. (2.10) over the nth-order expansion terms of the Mayer function [cf. Eq. (2.15)]. Specifically, one has for $n>1$

$$\tilde{u}_{lm}^{(n)}=-\frac{1}{2\beta}\frac{1}{4\pi^2 n!}(-\beta)^n\int_{\sigma}^{\infty}dr_{12}\frac{1}{r_{12}^{3n-2}} \times\int d\omega_1 d\omega_2 d\omega_{12}\mathcal{P}_l(\cos\theta_1)\mathcal{P}_m(\cos\theta_2) \times\tilde{\Phi}_{112}^n(\omega_1,\omega_2,\omega_{12}). \tag{2.19}$$

The case $n=1$ requires special care, since the integrand of $\tilde{u}_{lm}^{(1)}$ contains the dipolar potential itself and is therefore long ranged. As shown in a detailed analysis in Ref. [19], the result of this integration depends on the shape of the sample. For the shape of interest here, that is, an ellipsoidal volume inhibiting domain formation, the result of the integration is

$$\tilde{u}_{11}^{(1)}=-\frac{8\pi}{27}. \tag{2.20}$$

The remaining integrals in the $(n>1)$ coefficients (2.19) can be solved more straightforwardly. To this end one expresses the Legendre polynomials in spherical harmonics

$$\mathcal{P}_l(\cos\theta)=\sqrt{\frac{4\pi}{2l+1}}Y_{l0}(\omega), \tag{2.21}$$

and calculates the nth power of Φ_{112} by applying the product rule for rotational invariants **(**see Eq. (B8) in Ref. [19]**)** iteratively. Using then the orthogonality of the spherical harmonics [31] and the relation

$$C(l_1 l_2 0;000)=(-1)^l(2l+1)^{-1/2}\delta_{l_1 l_2} \tag{2.22}$$

(see Eq. (A.157) in Ref. [31]**)**, $\delta_{l_1 l_2}$ being the Kronecker symbol, one finds that

$$\tilde{u}_{lm}^{(n)}=0, \quad (l\neq m). \tag{2.23}$$

As a consequence, the quadratic expression for F^{dip} in Eq. (2.16) becomes diagonal in l, that is,

$$\frac{F^{\mathrm{dip}}}{\mathcal{V}}=\sum_{ab}\rho_a\rho_b\sum_{l=0}^{\infty}u_{ab,l}\alpha_{a,l}\alpha_{b,l}, \tag{2.24}$$

where

$$u_{ab,l}=\sum_{n=1}^{\infty}u_l^{(n)}(m_a m_b)^n, \tag{2.25}$$

and the $u_l^{(n)}$ are given by Eq. (2.19) with $l=m$.

In practice one has to truncate the expansion (2.15) of the Mayer function at a finite value $n_{\max}$. A truncation at $n_{\max}=1$ would imply that the expansion of the Mayer function reduces to the linear term, i.e., to the dipolar potential itself.

TABLE I. Numerical values of the $u_l^{(n)}$ for $l,n \leqslant 4$

	$n=1$	$n=2$	$n=3$	$n=4$
$l=0$	0	$-\frac{8\pi}{3}\frac{\beta}{3\sigma^3}$	0	$-\frac{8\pi}{25}\frac{\beta^3}{9\sigma^9}$
$l=1$	$-\frac{8\pi}{27}$	0	$-\frac{16\pi}{225}\frac{\beta^2}{6\sigma^6}$	0
$l=2$	0	$-\frac{8\pi}{375}\frac{\beta}{3\sigma^3}$	0	$-\frac{32\pi}{6125}\frac{\beta^3}{9\sigma^9}$
$l=3$	0	0	$\frac{16\pi}{257\,25}\frac{\beta^2}{6\sigma^6}$	0
$l=4$	0	0	0	$-\frac{8\pi}{992\,25}\frac{\beta^3}{9\sigma^9}$

One can show that this corresponds to the usual mean-field approximation [27] where the pair distribution function g is set to one (and, consequently, $\alpha_{a,l>1}=0$). However, the major drawback of this approximation (in contrast to the *modified* mean-field approximation) is that the dipolar contribution F^{dip} to the free energy vanishes for isotropic phases, which is clearly unphysical. In this work we choose $n_{\max}=4$, the numerical values of the $u_l^{(n)}$ for $l,n\leqslant 4$ are given in Table I.

B. Equilibrium configurations and phase equilibria

In order to locate phase coexistences it is generally more convenient to employ the grand canonical ensemble involving the chemical potentials μ_a (instead of the densities ρ_a) as thermodynamic variables. The grand free energy density functional is given by

$$\frac{\Omega}{\mathcal{V}} = \frac{F^{\mathrm{id}}+F^{\mathrm{hs}}}{\mathcal{V}} + \sum_{ab}\rho_a\rho_b\sum_{l=0}^{\infty}u_{ab,l}\alpha_{a,l}\alpha_{b,l} - \sum_a \mu_a\rho_a. \tag{2.26}$$

Ω becomes minimal for the equilibrium configuration $[\rho_a,\overline{\alpha_a}(x)]$ corresponding to the set $(\mu_a,T,\mathcal{V})$. This principle leads to the following Euler-Lagrange equations for the singlet densities

$$\frac{\partial(\Omega/\mathcal{V})}{\partial\rho_a}=0, \quad \frac{\delta(\Omega/\mathcal{V})}{\delta\overline{\alpha_a}(x)}=0. \tag{2.27}$$

Employing now the functional (2.26), the first member of Eq. (2.27) yields the conditions

$$\frac{\partial}{\partial\rho_a}\left(\frac{F^{\mathrm{id}}+F^{\mathrm{hs}}}{\mathcal{V}}\right)+2\sum_b\rho_b\sum_{l=0}^{\infty}u_{ab,l}\alpha_{a,l}\alpha_{b,l}-\mu_a=0. \tag{2.28}$$

The minimization with respect to the orientational distribution $\overline{\alpha_a}(x)$ has to be performed obeying the norm condition in Eq. (2.4). Solving the resulting expression with respect to the orientational parameters $\alpha_{a,l}$ one obtains

$$\alpha_{a,l}=\frac{2l+1}{2}\frac{\int_{-1}^{1}dx\mathcal{P}_l(x)\exp\left[-\sum_b\beta\rho_b\sum_{i=1}^{\infty}(2i+1)u_{ab,i}\alpha_{b,i}\mathcal{P}_i(x)\right]}{\int_{-1}^{1}dx\,\exp\left[-\sum_b\beta\rho_b\sum_{i=1}^{\infty}(2i+1)u_{ab,i}\alpha_{b,i}\mathcal{P}_i(x)\right]}. \tag{2.29}$$

The coupled equations (2.28) and (2.29) can be solved numerically by employing a multidimensional Newton-Raphson algorithm, yielding the equilibrium configuration for given $(\mu_a,T,\mathcal{V})$. In order to identify *coexisting states* at given chemical potentials μ_{A} and μ_{B}, we combine Eqs. (2.28) and (2.29) with a further equation reflecting that the pressures $p=-\Omega^{\mathrm{eq}}(\mu_{\mathrm{A}},\mu_B,T)/\mathcal{V}=-\Omega[\rho_a^{\mathrm{eq}},\overline{\alpha}_a^{\mathrm{eq}}(x)]/\mathcal{V}$ of both states have to be equal as well.

C. Critical line

In their MMF study of the phase behavior of one-component dipolar fluids, Groh and Dietrich [19] have shown that these systems exhibit at sufficiently high temperatures a critical line $\rho_{\mathrm{fc}}(T)$ at which the system undergoes a second-order transition from an isotropic ($\rho<\rho_{\mathrm{fc}}$) into a ferroelectric ($\rho>\rho_{\mathrm{fc}}$) state. Based on these results we expect similar behavior to occur as well in our dipolar mixtures, where, however, the critical line will also depend on the composition. In order to get an analytical expression for this critical line we expand the orientational part of the free energy,

$$\frac{\Delta F}{\mathcal{V}}=\sum_a\frac{\rho_a}{\beta}\int_{-1}^{1}dx\overline{\alpha_a}(x)\ln(2\overline{\alpha_a}(x))+\sum_{ab}\rho_a\rho_b\sum_{l=1}^{\infty}u_{ab,l}\alpha_{a,l}\alpha_{b,l}, \tag{2.30}$$

for small deviations from the isotropic state, i.e., small $\alpha_{a,l}$. A Taylor expansion of the entropic part of $\Delta F/\mathcal{V}$ up to second order yields

$$\sum_a \frac{\rho_a}{\beta}\int_{-1}^{1} dx\,\overline{\alpha}_a(x)\ln(2\overline{\alpha}_a(x))$$
$$= \sum_a \frac{\rho_a}{\beta}\int_{-1}^{1} dx\left(\frac{1}{2}+\sum_{l=1}^{\infty}\alpha_{a,l}\mathcal{P}_l(x)\right)$$
$$\times\ln\left(1+2\sum_{l=1}^{\infty}\alpha_{a,l}\mathcal{P}_l(x)\right)$$
$$= \sum_a \frac{\rho_a}{\beta}\sum_{l=1}^{\infty}\left(\frac{2}{2l+1}\right)\alpha_{a,l}^2+\cdots, \qquad (2.31)$$

where we used the expansion (2.5) of the orientational distribution function, the expansion $(1/2+\xi)\ln(1+2\xi)=\xi+\xi^2+O(\xi^3)$, and the orthogonality of the Legendre polynomials. The dots in Eq. (2.31) stand for higher order terms. Using Eqs. (2.30) and (2.31) $\Delta F/\mathcal{V}$ can be rewritten as

$$\frac{\Delta F}{\mathcal{V}} = \sum_{l=1}^{\infty}\sum_{ab}(\mathbf{M}_l)_{ab}\alpha_{a,l}\alpha_{b,l}, \qquad (2.32)$$

where the elements of the symmetric matrices $\mathbf{M}_l$ are defined by

$$(\mathbf{M}_l)_{ab} = \rho_a\rho_b u_{ab,l} + \delta_{ab}\frac{\rho_a}{\beta}\left(\frac{2}{2l+1}\right) \quad (l\geqslant 1). \qquad (2.33)$$

For the following analysis it is more convenient to rewrite the $(\mathbf{M}_l)_{ab}$ in terms of the total density $\rho=\rho_A+\rho_B$ and the concentrations $c_A=\rho_A/\rho$, $c_B=\rho_B/\rho=1-c_A$. This yields

$$\mathbf{M}_l = \begin{pmatrix} \rho^2 c_A^2 u_{AA,l} + \dfrac{2}{2l+1}\dfrac{\rho c_A}{\beta} & \rho^2 c_A c_B u_{AB,l} \\ \rho^2 c_B c_A u_{BA,l} & \rho^2 c_B^2 u_{BB,l} + \dfrac{2}{2l+1}\dfrac{\rho c_B}{\beta} \end{pmatrix}. \qquad (2.34)$$

The rigorous condition for the isotropic configuration to be stable is that $\mathbf{M}_l$ is positive definite [i.e., both eigenvalues $\lambda_i(i=1,2)$ are positive] for every l. However, our numerical analysis has shown that it is in fact enough to consider only the "leading" matrix $\mathbf{M}_1$, since the $\mathbf{M}_{l>1}$ are always positive definite as long as this is true for $\mathbf{M}_1$. As a consequence, the condition for criticality is that $\mathbf{M}_1$ becomes positive semidefinite, i.e.,

$$\lambda_1 = 0, \quad \lambda_2 > 0. \qquad (2.35)$$

Applying this criterion to the matrix at hand [cf. Eq. (2.34) with $l=1$] one finds that an asymmetric mixture ($\Gamma<1$)) with given concentration $0<c_A<1$ and given temperature T orders spontaneously at densities above the critical density

$$\rho_{\mathrm{crit}} = \frac{-\frac{2}{3}(c_A u_{AA,1}+c_B u_{BB,1}) - \frac{2}{3}\sqrt{(c_A u_{AA,1}+c_B u_{BB,1})^2 - 4c_A c_B(u_{AA,1}u_{BB,1}-u_{AB,1}^2)}}{2\beta c_A c_B(u_{AA,1}u_{BB,1}-u_{AB,1}^2)}. \qquad (2.36)$$

The limiting cases $c_A\to 1$ (pure A fluid) and $c_A\to 0$ (pure B fluid) have to be treated with special care, since both nominator and denominator in Eq. (2.36) vanish if $c_A=0,1$ (i.e., $c_B=1,0$). However, applying the rule of de l'Hospital to Eq. (2.36) yields

$$\rho_{\mathrm{crit}} = -\frac{2/3}{\beta c_A u_{AA,1}+\beta(1-c_A)u_{BB,1}}, \quad (c_A\to 0,1), \qquad (2.37)$$

which is equivalent to the known result Eq. (7.10) in Ref. [19]. For the other limiting case, that is, mixtures with $\Gamma=1$ (and therefore $u_{AA,1}=u_{AB,1}=u_{BB,1}$), condition (2.35) directly leads to the one-component case, regardless of the concentration c_A.

Additional information on the mixture's behavior at the critical line can be obtained via an analysis of the eigenvectors of $\mathbf{M}_1$ directly at ρ_{crit}. Under these conditions, the eigenvector $\boldsymbol{\alpha}=(\alpha_{A,1},\alpha_{B,1})^{\mathsf{T}}$ associated to the vanishing eigenvalue λ (which causes the determinant to go to zero) is given as

$$\boldsymbol{\alpha} = \begin{pmatrix} -(\mathbf{M}_1)_{AB} \\ (\mathbf{M}_1)_{AA} \end{pmatrix}. \qquad (2.38)$$

Interpreting λ as a vanishing "restoring force" against fluctuations with direction $\boldsymbol{\alpha}$ [32,33], it follows that this direction can give information on the *character* of the phase transition in the space of order parameters. In that sense one concludes from Eq. (2.38) that while crossing the critical line, the system will order such that the leading order parameters $\alpha_{A,1}$ and $\alpha_{B,1}$ are coupled by

$$\frac{\alpha_{B,1}}{\alpha_{A,1}} = \frac{P_{B,1}}{P_{A,1}} = \frac{(\mathbf{M}_1)_{AA}}{-(\mathbf{M}_1)_{AB}}. \qquad (2.39)$$

Inspection of the matrix elements at the critical line shows that $(\mathbf{M}_1)_{AB}$ is always negative whereas $(\mathbf{M}_1)_{AA}$ is positive. Therefore, Eq. (2.39) implies that the isotropic-to-ferroelectric transition in our dipolar mixtures is always characterized by a *parallel* ordering ($\alpha_{B,1}/\alpha_{A,1}=P_{B,1}/P_{A,1}>0$) of *both* species, with the ratio between the order parameters given by Eq. (2.39).

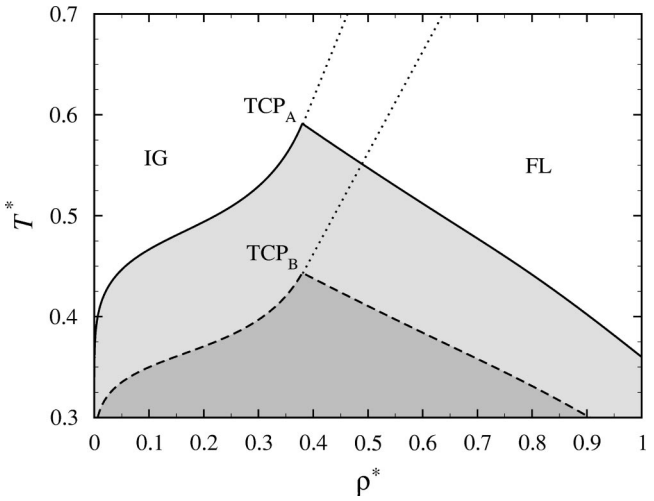

FIG. 1. Phase diagrams of two (decoupled) one-component fluids with interaction ratio $\Gamma=0.75$ in the density-temperature plane ($T^*=k_BT\sigma^3/m_A^2, \rho^*=\rho\sigma^3$). For explanation of the lines and symbols, see main text.

III. RESULTS

A. Reduced quantities

In order to characterize the phase behavior of the system we use the following reduced quantities: the temperature $T^*=k_BT\sigma^3/m_A^2$, measuring thermal energy versus the dipolar pair energy for two tangent spheres of species *A* in a parallel side-by-side configuration, the densities $\rho_a^*=\rho_a\sigma^3$ and the chemical potentials $-\mu_a^*=\ln(\Lambda_a^3/\sigma^3)-\beta\mu_a$. The total reduced density and the concentration of species *A* then follow as $\rho^*=\rho_A^*+\rho_B^*$ and $c_A=\rho_A/\rho$. Finally, the different dipolar couplings in the mixture are specified by the parameter $\Gamma=m_B^2/m_A^2$, measuring the ratio of the dipolar coupling strengths within species *A* and *B*, respectively. It is sufficient to consider mixtures with $0\leqslant\Gamma\leqslant 1$ (the behavior at larger Γ then simply follows from interchanging *A* and *B*).

B. Background: The one-component case

Before considering dipolar mixtures it is instructive to briefly discuss the MMF phase behavior of one-component dipolar hard-sphere fluids (previously obtained in Ref. [19,20]). Results are shown in Fig. 1 where the full lines combined with the upper dotted line correspond to the phase diagram of a pure *A* fluid in the density-temperature plane. Disregarding any solid structures (which are not captured by the present approach) there are two phases involved, an isotropic gas (IG) with zero orientational order parameters ($\alpha_{A,l>1}=0$) appearing at low and intermediate densities and a ferroelectric liquid (FL) with $\alpha_{A,l>1}>0$ appearing at higher number densities. Below the temperature $T^*_{\mathrm{TCP}_A}$ related to the *tricritical point* (TCP) of the pure *A* fluid, the transition between the isotropic and the ferroelectric phase is characterized by large jumps both in density (see gray regions in Fig. 1) and in the order parameters $\alpha_{A,l>1}$. Increasing T^* towards $T^*_{\mathrm{TCP}_A}$, the differences between coexisting phases vanish, and for temperatures above $T^*_{\mathrm{TCP}_A}$ the transition from the isotropic to the ferroelectric fluid is continuous in all order parameters, resulting in a *critical line* as described by Eq. (2.37) for $c_A\to 1$.

It may be noted that the MMF theory does not capture the full fluid phase behavior in the sense that dipolar chain and network formation processes observed in computer simulation studies of dilute, strongly coupled dipolar systems [10–12,14] do not appear. On the other hand, a feature correctly reproduced by the MMF theory is the absence of an ordinary condensation transition between an isotropic gas and an isotropic liquid in dipolar hard sphere systems without any additional (isotropic) attractive interactions [13,14]. Finally, the spontaneously polarized fluid phases as predicted by the MMF theory have also been observed in computer simulations [15–18], and integral equation studies [22], even though a comparison of ferroelectric transition temperatures indicates that the MMF theory seriously overestimates the tendency for long-range ferroelectric order (as one might have expected).

Since phase diagrams in the density-temperature plane are easy to understand we will employ this type of representation also in our discussion of *mixtures* of *A* and *B* particles with interaction ratio Γ. The density axis will then be the *total density* ρ^* of the system. In order to control the *composition* of the mixture, say, the concentration of *A* particles c_A, we will employ the difference between the chemical potentials, specifically the parameter $\Delta\mu^*\equiv\mu_B^*-\mu_A^*$. In this way the limit $\Delta\mu^*\to-\infty$ corresponds to a situation where *B* particles are completely expelled from the system at all temperatures ($c_A=1$ and $\rho^*=\rho_A^*$), yielding the density-temperature phase diagram of a pure *A* fluid shown in Fig. 1. The opposite behavior is found in the limit $\Delta\mu^*\to\infty$ where $c_A=0$ (i.e., $\rho^*=\rho_B^*$) at all temperatures and the phase diagram reduces to that of a pure *B* fluid. The latter is indicated by the dashed set of lines in Fig. 1. The phase diagram and specifically the reduced tricritical temperature $T^*_{\mathrm{TCP}_B}$ of a pure *B* fluid can be obtained by *scaling* the temperatures of the *A* system by a factor of Γ: since $\beta u_{AA}^{\mathrm{dip}}(\mathbf{r}_{12},\omega_1,\omega_2)=(\beta/\Gamma)u_{BB}^{\mathrm{dip}}(\mathbf{r}_{12},\omega_1,\omega_2)$, a configuration $[\rho,\overline{\alpha(x)}]$ will be stable for a pure *B* fluid at a temperature ΓT^*, if it is a stable configuration for a pure *A* fluid at the temperature T^*.

C. True mixtures

As reasoned in Sec. III B the chemical potential difference $\Delta\mu^*$ can be used as a "tuning" parameter controlling the change of the density-temperature phase diagram of a dipolar mixture with fixed Γ from the pure *A* to the pure *B* case ($\Delta\mu^*\to\pm\infty$). Investigating now "true" dipolar mixtures with finite values of $\Delta\mu^*$ for a range of interaction parameters $0\leqslant\Gamma\leqslant 1$ it turns out that one can distinguish *three* regimes of Γ, which differ in the types of phase behavior encountered by the systems on their way from *A* to *B*. Characteristic features of each regime are discussed in the following paragraphs for exemplary values of Γ. For reasons discussed above we start by considering phase diagrams in the density-temperature (and concentration-temperature) plane. In order to better understand the "global picture," however, we

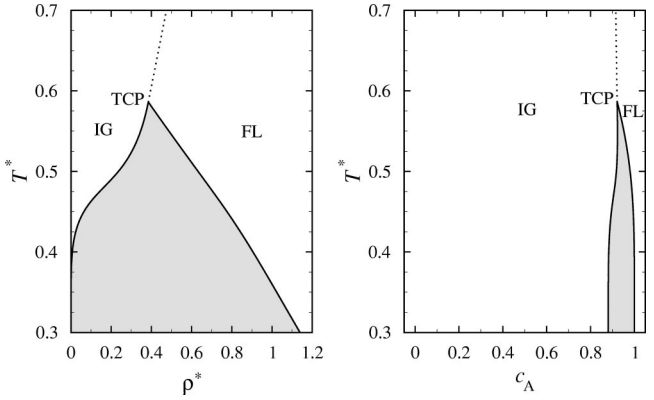

FIG. 2. Phase diagrams of a dipolar hard-sphere mixture with interaction ratio $\Gamma=0.75$ and chemical potential difference $\Delta\mu^*=-2.0$ in the density-temperature plane (left) and the concentration-temperature plane (right).

present in Sec. III D additional diagrams in the density-concentration plane.

1. $\Gamma=0.75$*: Tricriticality for every* c_A

The case $\Gamma=0.75$ is typical for systems where the dipolar coupling strengths within and in between the *A* and *B* species are still quite similar. Increasing $\Delta\mu^*$ from its lower limit $-\infty$ (pure *A* fluid), one encounters at first the phase behavior displayed in the two parts of Fig. 2. Values of the densities related to coexisting and critical states [see left-hand side (lhs) of Fig. 2] are still very similar to the pure case, and the only significant feature identifying the system as a mixture is the appearance of small changes of *composition* at the isotropic-ferroelectric transition. The amount of these changes can be seen from the right-hand side (rhs) of Fig. 2 displaying the values of the parameter c_A related to coexisting and critical states. Due to the small values of $\Delta\mu^*$ both coexisting phases are clearly dominated by *A* particles ($c_A \gg 0.5$), but the phase even more saturated in *A* is the ferroelectric phase. This is due to the stronger dipolar coupling between *A* particles and the higher density of the ferroelectric phase. Both effects yield a stronger effective (mean) field. The typical behavior of the leading orientational order parameters $P_{A,1}$ and $P_{B,1}$ upon crossing a critical line is displayed in Fig. 3 for an exemplary temperature. Clearly, the two order parameters have the same sign, which is consistent with the analysis in Sec. II C and implies that the two species order *parallel*. From a physical point of view, we understand this feature as a consequence of the "cross" effective field experienced by the (more weakly coupled) *B* particles as soon as the *A* particles start to order. The other curve in this figure represents the behavior of the concentration c_A, showing that the composition of the mixture varies *continuously* (as does the total density) when the system enters the ferroelectric state.

Changes in the phase diagrams induced by further increase of the chemical potential difference, i.e., by a stronger and stronger favoring of the (more weakly coupled) *B* species are depicted in Figs. 4 and 5, respectively. Specifically, from Fig. 4 it is seen that the general topology involving two

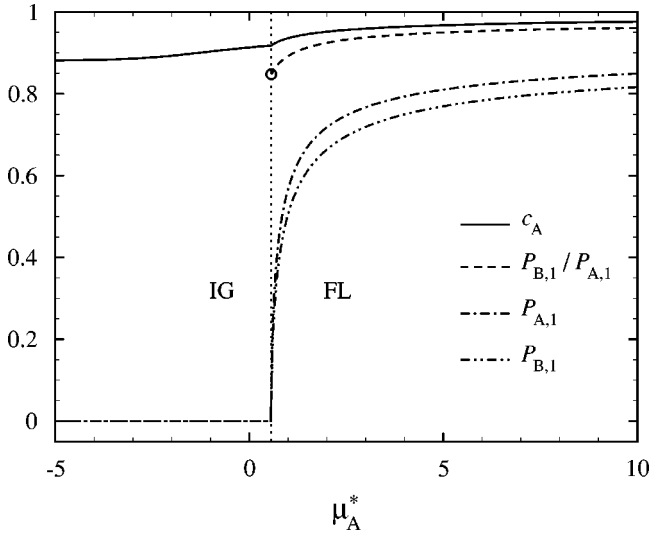

FIG. 3. Polarization order parameters and composition as functions of μ_A^* upon crossing the critical line ($\Gamma=0.75$, $\Delta\mu^*=-2.0$, $T^*=0.65>T_{TCP}^*$). The upper dashed line shows the numerically obtained values for the ratio $P_{B,1}/P_{A,1}$, which coincides at the critical line with the analytically obtained value (see circle) from Eq. (2.39).

fluid phases is kept as long as $\Delta\mu^*$ is not too high. The main effect of changing $\Delta\mu^*$ in this regime is that the temperature related to the TCP monotonically decreases, accompanied by a decrease of the corresponding values of c_A and an increase of the composition differences between coexisting phases below T_{TCP}^*. Only at very high (but still finite) values of $\Delta\mu^*$ (Fig. 5) one encounters a new topology involving, in addition to the TCP, a *critical point* (CP) separating two ferroelectric phases with different densities. However, as seen from the rhs of Fig. 5 the most significant difference between the coexisting phases is in fact the large gap in the composition. We thus can conclude that the phase transition within the ferroelectric fluid state is essentially a *demixing* transition, driven by high values of $\Delta\mu^*$ which favors the *B* species so strongly that coexistence of a B-rich ferroelectric liquid (FL_B) with an even denser *A*-rich ferroelectric liquid (FL_A) becomes possible.

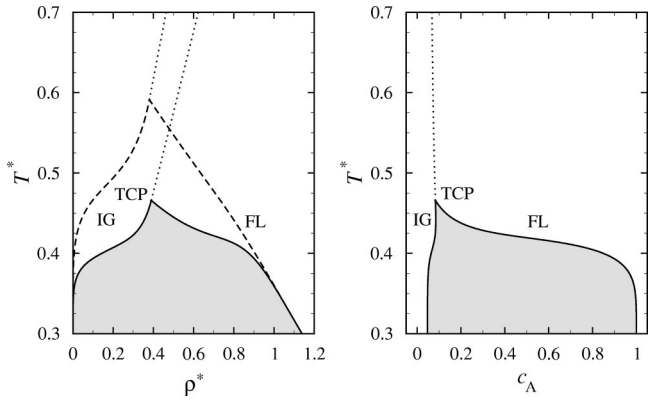

FIG. 4. Same as Fig. 2, but for $\Delta\mu^*=3.0$. The density-temperature diagram contains the results for the pure *A* fluid as a reference.

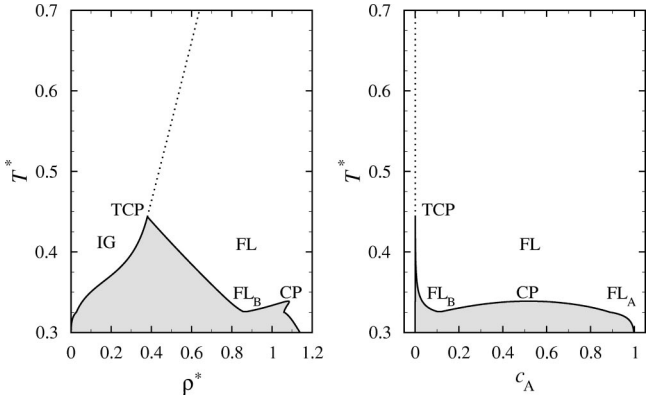

FIG. 5. Same as Fig. 2, but for $\Delta\mu^*=8.0$.

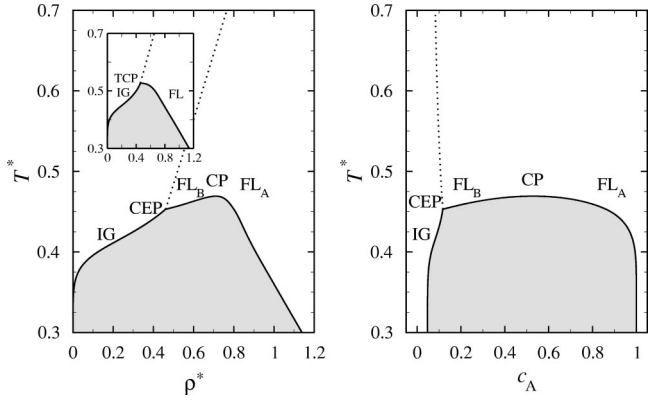

FIG. 6. Phase diagrams for $\Gamma=0.60$ and $\Delta\mu^*=3.0$. The inset on the lhs additionally contains the density-temperature diagram at $\Delta\mu^*=1.3$.

It is clear that the demixing CP must disappear again when $\Delta\mu^*$ is pushed towards even higher values where the behavior of the mixture approaches *per definitionem* that of the pure *B* fluid. Practically, this happens such that the temperature of the triple point (IG)-(FL_B)-(FL_A) moves towards smaller and smaller values, while the densities of the coexistence (FL_B)-(FL_A) are getting higher and higher and eventually leave the fluid phase regime. Finally the density-temperature phase diagram of the pure *B* fluid involving only a TCP results (cf. Fig. 1).

2. $\Gamma=0.60$*: Appearance of critical end points*

We now turn to more asymmetric mixtures with smaller coupling ratios, taking the case $\Gamma=0.60$ as an example. Starting again from the pure *A* fluid and increasing $\Delta\mu^*$ one finds at first phase diagrams containing only a TCP (IG)-(FL), similar to those depicted in Figs. 2 and 4 for the case of mixtures with more symmetric dipolar couplings. Contrary to the latter systems, however, where further increase of $\Delta\mu^*$ yields simultaneous appearance of both a TCP and a (demixing) critical point FL_A-FL_B at substantially higher densities (cf. Fig. 5), increase of $\Delta\mu^*$ at $\Gamma=0.60$ favors the demixing tendency so strongly that a $CP_{FL_B\text{-}FL_A}$ develops at temperatures and densities in the *immediate vicinity* of the TCP. As a result, the TCP becomes *unstable* and eventually changes into a *critical end point* (CEP) where the ferroelectric critical line meets the (IG)-(FL_A) coexistence at temperatures below the CP. Density-temperature phase diagrams corresponding to the scenario immediately before and after the transformation of the TCP into a CEP are displayed in the lhs of Fig. 6. The concentration diagram on the rhs moreover shows that the (IG)-(FL_A) transition at temperatures around T_{CEP} involves large jumps in the *composition*. This again identifies the appearance of a CEP plus a CP within the ordered phase as a phenomenon, which is rather driven by the combined tendencies of the system to order ferroelectrically and to demix, than by its tendency to just condensate at low temperatures.

In this context it is worth to note that a similar phase behavior involving a CEP plus a critical point at *higher* number densities has been observed for other complex fluids where "ordering" tendencies dominate the phase behavior. Examples are the paramagnetic-ferromagnetic CEP (plus a magnetic CP) observed in a Heisenberg spin fluid with purely repulsive spherical interactions [27,34], and spatially confined symmetric binary square-well mixtures where the presence of walls stabilizes demixing transitions [36].

Given the disappearance of the TCP in favor of a CEP (Fig. 6) it is interesting to see how the system's phase behavior changes back to that of the pure *B* system (involving only a TCP) upon further increasing of $\Delta\mu^*$. An intermediate situation encountered on this way is presented in Fig. 7. It is seen that the demixing CP has now moved to densities outside the range typical for fluid states, such that the density-temperature diagram displayed in Fig. 7 contains only first-order (FL_B)-(FL_A) transitions. Moreover, the CEP has changed back into a TCP, yielding again a *triple point* (IG)-(FL_B)-(FL_A). Further increase of chemical potential differences yields smaller and smaller triple point temperatures (see the dashed lines in Fig. 7 as an example) and finally the phase diagram of the pure *B* fluid.

3. Strongly asymmetric mixtures: Nonmonotonic behavior of (tri)critical points

From a topological point of view, mixtures with smaller coupling ratios ($\Gamma\leqslant 0.5$) were found to display essentially

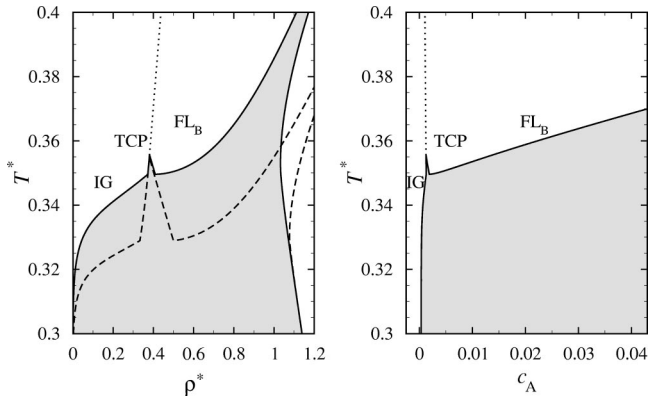

FIG. 7. Same as Fig. 6 but for $\Delta\mu^*=8.0$. The dashed lines on the lhs correspond to the density-temperature diagram at an even higher value of $\Delta\mu^*=10.0$.

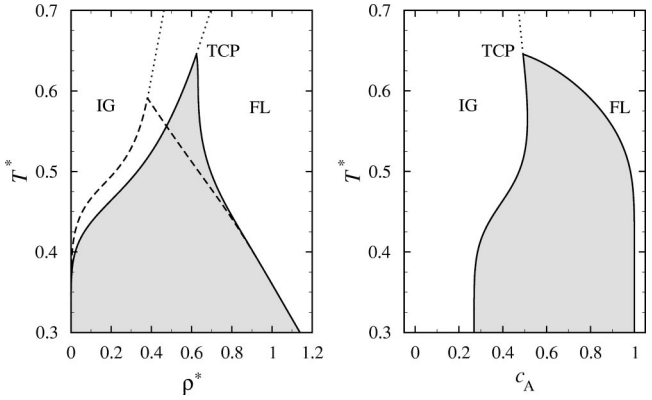

FIG. 8. Phase diagrams for $\Gamma=0.40$ and $\Delta\mu^*=1.0$. The ρ^*-T^* representation (left) contains the results for $\Delta\mu^*=-\infty$ (pure A fluid) as a reference.

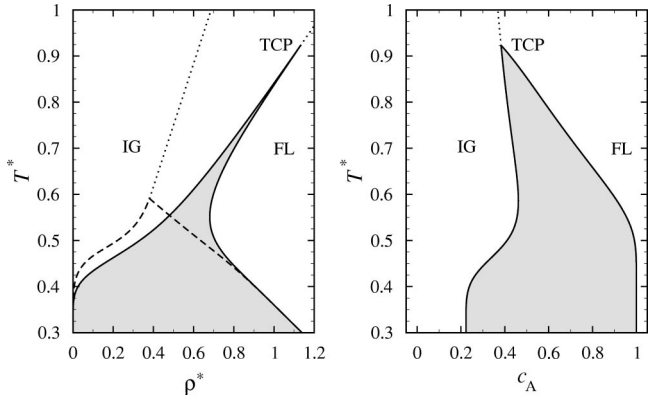

FIG. 10. Phase diagrams for $\Gamma=0.30$ and $\Delta\mu^*=1.25$. The ρ^*-T^* diagram (left) contains the results for a pure A fluid as a reference.

the same types of phase diagrams already discussed in the two previous paragraphs. However, closer inspection reveals some subtle, yet significant differences, the first of which occurs already at $\Gamma=0.40$ and concerns the $\Delta\mu^*$ dependence of the tricritical temperature. We recall that for the more symmetric mixtures, T^*_{TCP} monotonically *decreases* when the chemical potential difference is increased away from its limiting value $-\infty$ (i.e., the pure A fluid). This monotonic decrease is intuitively clear since the dipolar coupling within the B component is weaker, yielding a smaller and smaller tendency for ferroelectric ordering of the overall mixtures with increasing $\Delta\mu^*$. Having in mind this picture it is particularly surprising that, for $\Gamma=0.40$, the temperature related to the TCP at first *increases* when B particles are added to the mixture. This can be see from the density-temperature diagrams on the lhs of Fig. 8 and also from Fig. 9 where the $\Delta\mu^*$ dependence of the TCPs (or CEPs, respectively) is displayed for all Γ regimes. Figure 9 additionally shows that, at $\Gamma=0.40$, the tricritical temperature only starts to decrease again after the TCP has changed into a CEP. Similar behavior

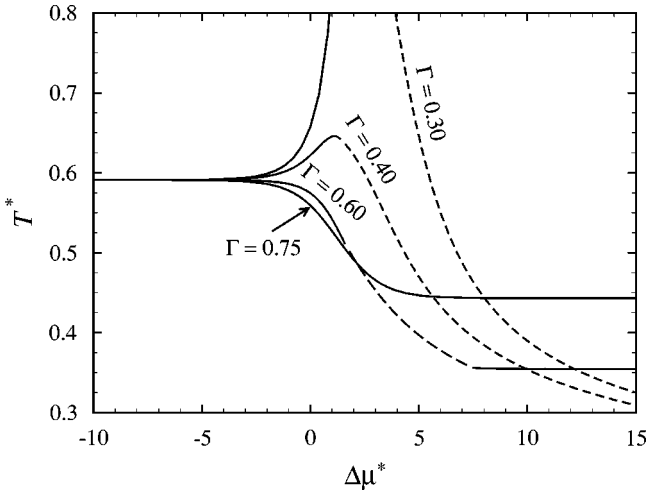

FIG. 9. Temperatures related to the tricritical points (or critical end points) of the mixtures as functions of the chemical potential difference for various values of Γ. Solid (dashed) parts of the lines correspond to TCPs (CEPs).

of the TCP/CEP temperature occurs for the most asymmetric mixtures considered, characterized by an interaction ratio $\Gamma=0.30$ [cf. Fig. 9]. We note, however, that for an intermediate range of $\Delta\mu^*$ the TCP/CEP appears at densities far *outside* the range of densities where one would expect fluid phases to be stable (and this is even more true for the densities related to demixing CPs). Specifically, given that both species in the present mixtures have the same diameter and given [16] that one-component fluids of DHS freeze at densities comparable to those of pure HS systems [36], i.e., $\rho^*\approx 0.95$, one expects similar freezing densities for the present mixtures. An exemplary MMF phase diagram (where solid phases are not taken into account) for a highly asymmetric mixture is depicted in Fig. 10, showing that tricriticality occurs at unphysical fluid densities in the vicinity of the close-packing limit. We can therefore expect that true mixtures of this type would display only first-order fluid-fluid transitions, with exceptions appearing at very large or very small values of $\Delta\mu^*$ (i.e., close to the pure cases).

D. The global picture

In order to round off our discussion of the MMF results we finally present some alternative representations of the phase behavior. Although these contain, of course, essentially the same information as do the two-dimensional phase diagrams displayed in Sec. III C, we found the additional diagrams displayed below particularly helpful in order to elucidate the differences of the mixture's phase behavior at different values of Γ.

We start with Fig. 9 which has been already referred to at the end of Sec. III C and shows the $\Delta\mu^*$ dependence of the temperature related to the TCP (or CEP, respectively) for all three Γ regimes. For the more symmetric mixtures corresponding to $\Gamma=0.75$ and $\Gamma=0.60$ this temperature monotonically *decreases* with increasing $\Delta\mu^*$, i.e., with increasing concentration of B particles, as expected due to their weaker dipolar coupling. The difference between these scenarios then consists in the absence or presence of a transformation TCP$\leftrightarrow$CEP at intermediate values of $\Delta\mu^*$ [cf. Secs. III C 1 and III C 2]. On the other hand, the more asymmetric mixtures ($\Gamma=0.4$ and 0.3), which tend to demix more strongly,

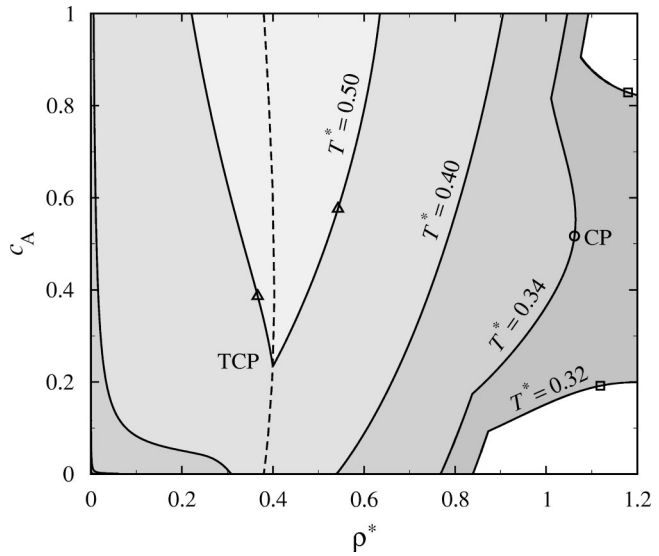

FIG. 11. Density-concentration phase diagram for a mixture with $\Gamma=0.75$ at various temperatures. The pair of triangles (squares) denotes coexisting states at $T^*=0.50/\Delta\mu^*=1.0(T^*=0.32/\Delta\mu^*=10.0)$. For further explanations, see main text.

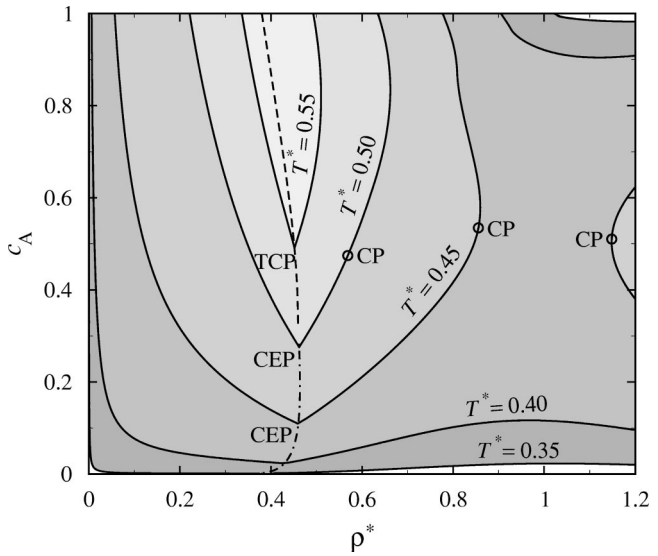

FIG. 12. Same as Fig. 11 but for $\Gamma=0.60$.

are characterized by a somewhat counterintuitive behavior of the tricritical temperature in the sense that T^*_{TCP} first *raises* and starts to decrease only after the TCP has changed into a CEP. The difference between these mixtures is then purely quantitative in the sense that at $\Gamma=0.3$ tricritical (and any other critical) behavior occurs at densities outside the fluid phase regime.

Besides the different behavior of $T^*_{\mathrm{TCP/CEP}}$, a further feature distinguishing the various mixture's phase behaviors is the topology and shape of the "three-dimensional" phase diagrams generated by plotting the (total) densities ρ^* and concentrations c_{A} corresponding to coexisting states of a given system (fixed Γ) at various temperatures. Examples are shown in Figs. 11–14. Solid lines are the two-phase coexistence lines (generated by varying $\Delta\mu^*$ at fixed T^*), whereas the dashed lines denote values of ρ^* and c_{A} related to the TCP/CEP. As a consequence, the crossing of these lines with the horizontals at $c_{\mathrm{A}}=1$ and $c_{\mathrm{A}}=0$ indicates the tricritical densities of a pure A or B fluid. We also note that, for each Γ, states on the rhs (lhs) of the dashed line in Figs. 11–14 correspond to ferroelectric (isotropic) states.

We start again with the Fig. 11 corresponding to nearly symmetric mixtures ($\Gamma=0.75$). It is seen that, for a broad range of densities and temperatures, the first-order isotropic-ferroelectric transition involves changes mainly in the density rather than in c_{A} (as shown exemplarily by the coexisting states denoted by the pair of triangles in Fig. 11) whereas demixing only comes into play at very high values of ρ^* (squares in Fig. 11). As a result, the line of tricritical points, which are characterized by significantly smaller densities than those associated to the demixing CP, remains essentially unaffected by the demixing transitions. This obviously changes when going to smaller interaction ratios where demixing becomes more favorable, as reflected in Fig. 12 both by the appearance of a CEP and by the (compared to Fig. 11) smaller densities and higher temperatures associated to the demixing critical points. Considering now even more asymmetric systems [cf. Fig. 13] one observes a yet new feature in the density-concentration diagram, namely a *closed* coexistence loop at a temperature $T^*=0.633$. Even though this temperature is higher than $T^*_{\mathrm{TCP_A}}$ the system still possesses a TCP. The appearance of the loop can be explained as follows: holding the temperature fixed and increasing $\Delta\mu^*$ from $\Delta\mu^*_{\mathrm{TCP}}$ one observes at first the development of a (IG)-(FL) coexistence (see pair of triangles), implying that the TCP must have moved towards higher temperatures. After the transformation TCP$\leftrightarrow$CEP the (IG)-(FL) coexistence then changes into a ($\mathrm{FL_B}$)-($\mathrm{FL_A}$) coexistence, as indicated by the pair of squares in Fig. 13. Upon further increase of $\Delta\mu^*$ the

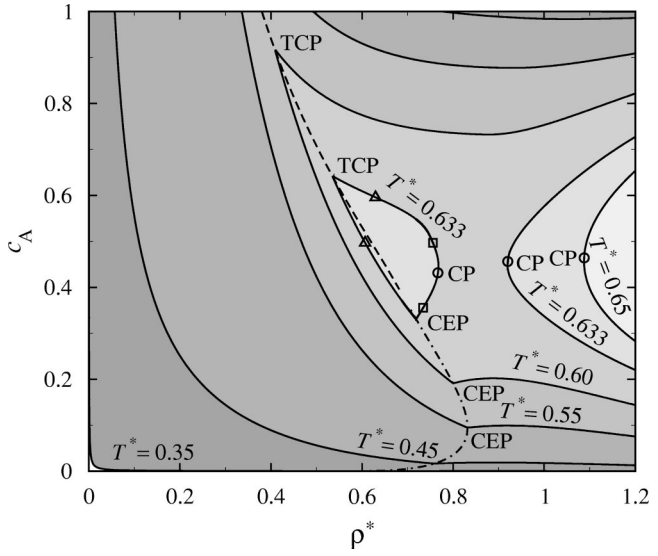

FIG. 13. Same as Fig. 11 but for $\Gamma=0.40$. The pair of triangles (squares) denotes coexisting states at $T^*=0.633$ and $\Delta\mu^*=1.0(\Delta\mu^*=1.75)$.

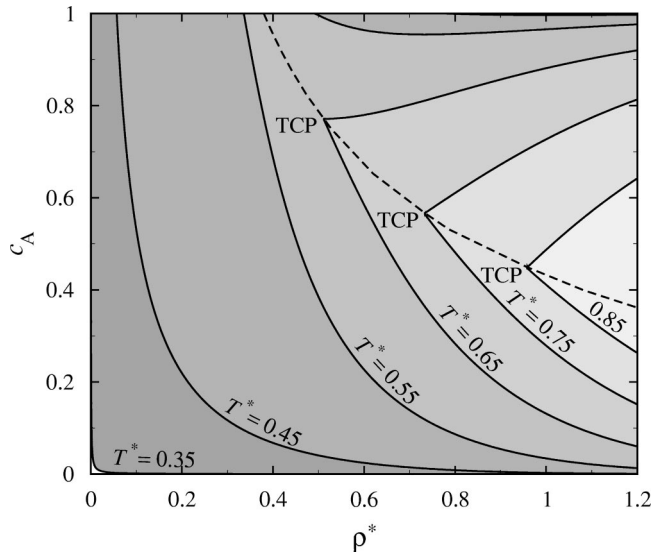

FIG. 14. Same as Fig. 11 but for $\Gamma=0.30$.

coexistence region finally closes at the demixing critical point. Therefore the appearance of such loops in the density-concentration diagrams just reflects nonmonotonic behavior of T^*_{TCP} upon varying $\Delta\mu^*$ (see discussion of Fig. 9). From this it is clear that the corresponding diagram for the most asymmetric mixtures considered here ($\Gamma=0.3$) should, in principle, also contain islands but it turns out that these are outside the physically meaningful density range (see discussion in Sec. III C 3). As a result one obtains a diagram dominated by first-order demixing transitions as displayed in Fig. 14.

IV. CONCLUSIONS

In this work we have explored the fluid-fluid phase behavior of asymmetric binary dipolar model mixtures in the framework of density functional theory in the modified mean-field (MMF) approximation. Phase diagrams have been obtained by minimizing the resulting free energy functional both for isotropic and for orientationally ordered fluid phases, supplemented by an appropriate stability analysis in order to locate critical lines. Despite the simplicity of our model system, where the two species differ only in their dipole moments, the resulting phase behavior turns out to be significantly richer than that of the one-component counterpart. One of the most surprising results was that even *tiny* differences between the dipole moments ($\Gamma=m_{\mathrm{B}}^2/m_{\mathrm{A}}^2\rightarrow 1$) result in the appearance of *demixing* transitions between two fluid phases of strongly different compositions, as signalled by the presence of a demixing critical point (CP). Whereas the corresponding densities are somewhat artificial (i.e., extremely high) as long as Γ is close to one, decrease of Γ more and more favors demixing until finally the corresponding CP appears at densities deep within the fluid phase regime. We stress, however, that these demixing CPs appeared always within the ferroelectrically ordered region, indicating that—within the MMF theory—asymmetric dipolar couplings alone are not enough do induce demixing already in the *isotropic* phase. In fact, we did not even find isotropic demixing transitions for the most asymmetric systems, that is, mixtures of dipolar and pure hard spheres ($\Gamma=0$). This finding is in contrast to recent integral equation [32,37] and computer simulation studies [38], which indicates that isotropic demixing in dipolar/hard-sphere mixtures without any dispersive interactions is essentially a *correlational* effect and in that sense far from being trivial. Given the discrepancy at $\Gamma=0$ one also concludes that the present MMF predications on the nature of demixing transitions at *finite* $\Gamma>0$ need to be carefully tested against simulations or other more sophisticated theoretical approaches. Work in this direction is currently in progress.

Beyond demixing, the other major effect of decreasing Γ in our MMF study is a significant shift of the isotropic-to-ferroelectric transition towards lower temperatures and/or larger densities relative to the one-component case. This suggests that spontaneously polarized phases in dipolar systems generally become strongly *destabilized* by nonuniformity in the dipole moments. In fact, a similar observation has also been made in a recent Monte Carlo study [7] where the degree of spontaneous polarization in strongly coupled dipolar hard-sphere mixtures with different dipole moments has found to be much smaller than in the pure system. In Ref. [7], no attempt has been made to determine the actual transition temperatures of the dipolar mixtures, but given the mean-field character of our theory we would expect the MMF predictions to be highly overestimated. Still, in view of the agreement on a qualitative level and given that calculations on the MMF level are much less time consuming, we feel encouraged to employ the present theory also to investigate other dipolar mixtures such as "binary ferrocolloids" with particles differing not only in their dipole moments, but also in their sizes. We note that the present approach could also be applied to other mixtures with angle-dependent interactions such as Heisenberg fluid mixtures or simple liquid crystal models. In fact, given the similarity of the results obtained within the MMF theory for single component Heisenberg [27] and dipolar fluids [19,20], we would expect the Heisenberg mixtures to display analogous features as we have found here, such as demixing transitions and destabilization of orientationally ordered phases.

ACKNOWLEDGMENTS

Sabine H. L. Klapp acknowledges financial support from the Deutsche Forschungsgemeinschaft through the Emmy-Noether Programm.

[1] M. Morillo, C. Denk, F. Sánchez-Burgos, and S. Antonio, J. Chem. Phys. **113**, 2360 (2000).
[2] M. Valiskó, D. Boda, J. Liszi, and I. Szalai, Phys. Chem. Chem. Phys. **3**, 2995 (2001).
[3] R. E. Rosensweig, *Ferrohydrodynamics* (Cambridge University Press, New York, 1985).
[4] *Ferrofluids, Magnetically Controllable Fluids and their Applications*, edited by S. Odenbach, Lecture Notes in Physics Vol. 594 (Springer-Verlag, Berlin, 2002).
[5] V. Russier and M. Douzi, J. Colloid Interface Sci. **162**, 356 (1994).
[6] A. O. Ivanov, J. Magn. Magn. Mater. **154**, 66 (1996).
[7] B. J. Costa Cabral, J. Chem. Phys. **112**, 4351 (2000).
[8] T. Kruse, A. Spanoudaki, and R. Pelster, Phys. Rev. B **68**, 054208 (2003).
[9] A. Bradbury, S. Menear, and R. W. Chantrell, J. Magn. Magn. Mater. **54**, 745 (1986).
[10] J.-J. Weis and D. Levesque, Phys. Rev. Lett. **71**, 2729 (1993).
[11] D. Levesque and J.-J. Weis, Phys. Rev. E **49**, 5131 (1994).
[12] J. M. Tavares, J.-J. Weis, and M. M. Telo da Gama, Phys. Rev. E **59**, 4388 (1999).
[13] J.-M. Caillol, J. Chem. Phys. **98**, 9835 (1993).
[14] M. E. van Leeuwen and B. Smit, Phys. Rev. Lett. **71**, 3991 (1993).
[15] J.-J. Weis, D. Levesque, and G. J. Zarragoicoechea, Phys. Rev. Lett. **69**, 913 (1992).
[16] J.-J. Weis and D. Levesque, Phys. Rev. E **48**, 3728 (1993).
[17] D. Wei and G. N. Patey, Phys. Rev. Lett. **68**, 2043 (1992).
[18] D. Wei and G. N. Patey, Phys. Rev. A **46**, 7783 (1992).
[19] B. Groh and S. Dietrich, Phys. Rev. E **50**, 3814 (1994).
[20] B. Groh and S. Dietrich, Phys. Rev. Lett. **72**, 2422 (1994).
[21] B. Groh and S. Dietrich, Phys. Rev. E **57**, 4535 (1998).
[22] S. Klapp and F. Forstmann, J. Chem. Phys. **106**, 9742 (1997).
[23] B. Groh and S. Dietrich, Phys. Rev. E **53**, 2509 (1996).
[24] B. Groh and S. Dietrich, Phys. Rev. E **55**, 2892 (1997).
[25] B. Groh and S. Dietrich, Phys. Rev. Lett. **79**, 749 (1997).
[26] N. F. Carnahan and K. E. Starling, J. Chem. Phys. **51**, 635 (1969).
[27] J. M. Tavares, M. M. Telo da Gama, P. I. C. Teixeira, J.-J. Weis, and M. J. P. Nijmeijer, Phys. Rev. E **52**, 1915 (1995).
[28] P. I. Teixeira and M. M. Telo da Gamma, J. Phys.: Condens. Matter **3**, 111 (1991).
[29] P. Frodl and S. Dietrich, Phys. Rev. A **45**, 7330 (1992).
[30] P. Frodl and S. Dietrich, Phys. Rev. E **48**, 3203 (1993).
[31] C. G. Gray and K. E. Gubbins, *Theory of Molecular Fluids*, The International Series of Monographs on Chemistry Vol. 1 (Clarendon, Oxford, 1984).
[32] X. S. Chen and F. Forstmann, Mol. Phys. **76**, 1203 (1992).
[33] X. S. Chen and F. Forstmann, J. Chem. Phys. **97**, 3696 (1992).
[34] J.-J. Weis, M. J. P. Nijmeijer, J. M. Tavares, and M. M. Telo da Gama, Phys. Rev. E **55**, 436 (1997).
[35] D. Woywod and M. Schoen, Phys. Rev. E **67**, 026122 (2003).
[36] W. G. Hoover and F. H. Ree, J. Chem. Phys. **49**, 3609 (1968).
[37] X. S. Chen, M. Kasch, and F. Forstmann, Phys. Rev. Lett. **67**, 2674 (1991).
[38] M. J. Blair and G. N. Patey, Phys. Rev. E **57**, 5682 (1998).